A non-competing pair of human neutralizing antibodies block COVID-19 virus binding to its receptor ACE2

Yan Wu[1,2,#,*], Feiran Wang[3,4,#], Chenguang Shen[3,5,#], Weiyu Peng[3,6,#], Delin Li[3,5,7,#], Cheng Zhao[3,8], Zhaohui Li[3,9], Shihua Li[3], Yuhai Bi[3,10], Yang Yang[5], Yuhuan Gong[3,10], Haixia Xiao[7], Zheng Fan[3], Shuguang Tan[3], Guizhen Wu[11], Wenjie Tan[11], Xuancheng Lu[12], Changfa Fan[13], Qihui Wang[3], Yingxia Liu[5], Chen Zhang[1],Jianxun Qi[3], George Fu Gao[3,*], Feng Gao[7,*], Lei Liu[5,*]

Affiliations:

[1]Department of Pathogen Microbiology, School of Basic Medical Sciences, Capital Medical University, Beijing, China.

[2]Research Network of Immunity and Health (RNIH), Beijing Institutes of Life Science, Chinese Academy of Sciences, Beijing, China

[3]CAS Key Laboratory of Pathogenic Microbiology and Immunology, Institute of Microbiology, Chinese Academy of Sciences, Beijing, China.

[4]School of Life Sciences, University of Science and Technology of China, Hefei, Anhui 230026, China.

[5]Shenzhen Key Laboratory of Pathogen and Immunity, Shenzhen Third People's Hospital, Shenzhen 518112, China.

[6]College of Veterinary Medicine, China Agricultural University, Beijing, China.

[7]Laboratory of Protein Engineering and Vaccines, Tianjin Institute of Industrial Biotechnology, Chinese Academy of Sciences, Tianjin, China

[8]Shanxi Academy of Advanced Research and Innovation, Taiyuan 030032, China

[9]University of Chinese Academy of Sciences, Beijing 100049, China

[10]Center for Influenza Research and Early Warning, Chinese Academy of Sciences (CASCIRE), Beijing 100101, China

[11]NHC Key Laboratory of Biosafety, National Institute for Viral Disease Control and Prevention, Chinese Center for Disease Control and Prevention, Beijing, China

[12]Laboratory Animal Center, Chinese Center for Disease Control and Prevention, Beijing, China

[13]Division of Animal Model Research, Institute for Laboratory Animal Resources, National Institutes for Food and Drug Control, Beijing, China

#These authors contributed equally.

*Correspondence: wuy@biols.ac.cn (Y.W.); gaofeng@tib.cas.cn (F.G.), gaof@im.ac.cn (G.F.G.), liulei3322@aliyun.com（L.L.）

Abstract

Neutralizing antibodies could be antivirals against COVID-19 pandemics. Here, we report the isolation of four human-origin monoclonal antibodies from a convalescent patient in China. All of these isolated antibodies display neutralization abilities in vitro. Two of them (B38 and H4) block the binding between RBD and vial cellular receptor ACE2. Further competition assay indicates that B38 and H4 recognize different epitopes on the RBD, which is ideal for a virus-targeting mAb-pair to avoid immune escape in the future clinical applications. Moreover, therapeutic study on the mouse model validated that these two antibodies can reduce virus titers in the infected mouse lungs. Structure of RBD-B38 complex revealed that most residues on the epitope are overlapped with the RBD-ACE2 binding interface, which explained the blocking efficacy and neutralizing capacity. Our results highlight the promise of antibody-based therapeutics and provide the structural basis of rational vaccine design.

One Sentence Summary: A pair of human neutralizing monoclonal antibodies against COVID-19 compete cellular receptor binding but with different epitopes, and with post-exposure viral load reduction activity.

Main Text: The COVID-19 caused by the novel coronavirus COVID-19 virus has become a global health crisis. The virus has spread worldwide, causing fever, severe respiratory illness and pneumonia(*1, 2*). Phylogenetic analysis indicates that the emerging pathogen is closely related to several bat coronaviruses and to severe acute respiratory syndrome coronavirus (SARS-CoV)(*3-5*). It is worth to note that COVID-19 virus appears to be more easily transmitted from person to person(*6*). To date,

59 however, no specific drugs or vaccines are available so far, except for several general
60 antiviral drugs (eg. Remdesivir and hydroxychloroquine, et al.) under clinical
61 investigation.

62 COVID-19 virus belongs to betacoronavirus genus, in which five human infected
63 pathogens are implicated(*7, 8*). Among them, SARS-CoV and Middle East respiratory
64 syndrome coronavirus (MERS-CoV) are two highly pathogenic viruses. As with other
65 coronaviruses, the spike glycoprotein (S) homotrimer on the COVID-19 virus surface
66 plays an essential role in receptor binding, triggering the cell membrane fusion for virus
67 entry. The S protein is a class I fusion protein and each S protomer consists of S1 and
68 S2 domains(*9*). The receptor binding domain (RBD) locates on the S1 region(*8*).
69 Previous studies revealed that COVID-19 virus infects host cells by using the same
70 receptor ACE2 as SARS-CoV for entry(*3, 10-12*), and the RBD undergoes hinge-like
71 conformational movements to engage ACE2 binding(*13*). Numerous neutralizing
72 antibodies targeting RBD of either SARS-CoV or MERS have been identified(*14-16*).
73 Therefore, screening the neutralizing antibodies against COVID-19 virus by using the
74 RBD protein is the priority strategy.

75 We expressed COVID-19 virus RBD protein as a bait to isolate the specific single
76 memory B-cells from peripheral blood mononuclear cells (PBMCs) of a convalescent
77 COVID-19 patient. The variable regions encoding the heavy chain and light chain were
78 amplified from single B cells, respectively, and were then cloned into pCAGGS vector
79 with the constant region to produce IgG1 antibodies as previous described(*17*). 17
80 paired B cell clones were amplified and 3 of which were identical (B5, B59 and H1).

81 To identify the binding abilities of these antibodies, the plasmids containing the paired
82 heavy chain and light chains were co-transfected into HEK 293T cells for monoclonal
83 antibodies (mAbs) production. The supernatants were then screened for binding to
84 COVID-19 virus RBD by Bio-Layer Interferometry (BLI) in OctetRED96, and an
85 irrelevant anti-SFTSV Gn antibody and a SARS-CoV specific antibody were used as
86 controls. The supernatants from four different antibodies (B5, B38, H2 and H4) exhibit
87 the binding abilities to COVID-19 virus RBD, but failed binding to SARS-CoV RBD
88 (Figure S1), suggesting that the epitope between SARS-CoV and COVID-19 virus
89 RBDs are immunologically distinct. The usage of both heavy chain (V_H) and light chain
90 (V_L) variable genes are listed in Table S1.

91 We then further measured the binding kinetics using surface plasmon resonance (SPR).
92 These four antibodies displayed various binding abilities to COVID-19 virus RBD,
93 with K_d ranging from 10^{-7} to 10^{-9} M (Figure1 A-D). H4 presented relatively higher
94 binding affinity, with K_d of 4.48 nM, while B5 displayed relatively weaker binding
95 affinity, with K_d of 305 nM. B38 and H2 bind to RBD, with K_d of 70.1 nM and 14.3
96 nM, respectively. We next studied the neutralizing activities against COVID-19 virus
97 virus (BetaCoV/Shenzhen/SZTH-003/2020). All these four antibodies exhibit
98 neutralizing activities, with IC_{50} values ranging from 0.177 μg/ml to 1.375 μg/ml
99 (Figure 2). B38 was the most potent antibody, followed by H4, H2 and B5. Combined
100 with the results of the competitive binding assay, it is suggested that different mAbs
101 may exert neutralizing activities through distinct mechanisms.

102 To evaluate the competition abilities of each antibody for blocking the binding between
103 viral RBD and ACE2, we performed the competition assay by using BLI in
104 OctetRED96 and a blocking assay by using fluorescence-activated cell sorting (FACS).
105 Specifically, the streptavidin biosensors labelled with biotinylated RBD were saturated
106 with antibodies, and then flowed through with the test antibodies in the presence of
107 soluble ACE2. B38 and H4 showed completely competition with ACE2 for the binding
108 to RBD. In contrast, B5 displayed partial competition, while H2 show no competition
109 with ACE2 for the RBD binding (Figure 1 E-H). The blocking assay by FACS
110 presented similar results. Specifically, the ACE2-EGFP proteins were presented on the
111 cell surface by transfection of ACE2-EGFP plasmid into HEK 293T cells, and then
112 stained with RBD-histag proteins (positive control) or the preincubated RBD-antibody
113 mixture. Both B38 and H4 can block the binding between RBD and ACE2 (Figure1I),
114 suggesting that the epitopes of these two antibodies locate on the RBD-ACE2 binding
115 interface. To determine whether B38 and H4 target the same epitope, the epitope
116 competition assay was performed with BLI. The viral RBD immobilized on the Ni-
117 NTA sensor was first saturated with B38 IgG and flowed through B38 IgG in the
118 presence or absence of H4 IgG, and vice versa. The result indicated that although RBD
119 was saturated with the first antibody, the second antibody can still bind to RBD,
120 suggesting that B38 and H4 recognize different epitopes on RBD with partial
121 overlapping (Figure1 J-K).
122 To explore the protection efficacy of B38 and H4 against challenge with COVID-19
123 virus *in vivo*, therapeutic study was performed. hACE2 transgenic mice were

124 administered with a single dose of 25 mg/kg of B38 or H4 12 hours after virus challenge.
125 The results revealed that the body weight of B38 group substantially decreased and
126 recovered at 3 days post infection (dpi) compared with PBS control group and H4 group
127 (Figure 3A). The viral RNA copies of lung tissue were also detected at 3 dpi. The
128 relative RNA copies change of both B38 group and H4 group were significantly lower
129 than that of the PBS group, with a reduction of 32.8% and 26% RNA copies change of
130 that in PBS group, respectively (Figure 3B). These results exhibit the identical trends
131 to the neutralization abilities.
132 To further elucidate the structural basis of the neutralization mechanisms of the
133 antibodies, we prepared both the RBD-B38 and RBD-H4 Fab complexes by incubating
134 the two proteins *in vitro* and then purified with a gel filtration column. Consistent with
135 the binding affinity between viral RBD and B38 or H4, the stable complex was obtained
136 (Figure S2). We therefore determined the crystal structure of B38 Fab with the viral
137 RBD at 1.9 Å resolution (Table S2). Three complementarity-determining regions
138 (CDRs) on the heavy chain (HCDR) and two CDRs on the light chain (LCDR) are
139 involved in interaction with the viral RBD (Figure 4A and B). The buried surface area
140 of heavy chain and light chain on the epitope is 713.9 Å and 497.7 Å, respectively.
141 There are 36 residues in viral RBD involved in the interaction with B38, of which 21
142 residues and 15 residues interact with heavy chain and light chain, respectively (Table
143 S3 and Figure 4B). Sequence alignment indicates that only 15 of the 36 residues in the
144 epitope (defined as residues buried by B38) are conserved between COVID-19 virus
145 and SARS-CoV (Figure 4D, 4F, and S3). This explains the specific reactivity of B38.

146 Hydrophilic interactions are the major interacting forces on the interface between B38
147 and viral RBD (Table S4). Further analysis of the interactions of the binding interface
148 reveals that the 470-loop of viral RBD plays an important role in binding to B38
149 HCDR1 loop (Figure 4G). The conformation of 470-loop is supported by Q474. In
150 contrast, the corresponding loop (460-loop) in SARS-RBD displays distinct
151 conformation due to the β-turn formed by P462 and G464, which is unfit for HCDR1
152 binding. S30 and S31 form hydrogen bonds to the side chain of K458, while the
153 corresponding residue H445 in SARS-CoV RBD loses the interactions (Figure 4G). For
154 the residues on contacting with the HCDR2, K417 is the only different residue between
155 two RBDs involved in the interactions. The corresponding residue V404 in the SARS-
156 CoV RBD loses the hydrogen bond to Y52, and the conformational change of the
157 threonine results in losing the interaction with Y58 side chain (Figure 4H). Notably, the
158 interactions between the side chains of two residues (Y100 and D103) on the HCDR3
159 and COVID-19 virus RBD are mediated by water molecules (Figure 4I). Specifically,
160 the oxygen atom on the hydroxyl group interacts with E484, F490, L492 and Q493 on
161 RBD via two water molecules. The side chain of D103 on the HCDR3 interacts with
162 Y489 through a water molecule. Residue R97 on the HCDR3 hydrogen bonds to the
163 side chains of both Y489 and N487. For the corresponding residues involved in the
164 interactions with HCDR3 in SARS-CoV RBD, four residues are not conserved (N487,
165 Y489, P491 and L492). P469 and W476 (corresponding residues F490 and E484 in
166 COVID-19 virus RBD) are two unconserved residues between these two RBDs. E484
167 provides a polar contact with Y100 through water molecule, while P469 and W476 in

168 SARS-CoV RBD are hydrophobic residues, which may be unsuitable for antibody
169 binding. By contrast, residues involved in the interactions with LCDR loops between
170 COVID-19 virus RBD and SARS-CoV RBD are more conserved (Figure 4J and K).
171 Although two residues involved in the binding to LCDR3 loop are different between
172 these two RBDs, they have the same properties (R403 and E406 in COVID-19 virus
173 RBD, the corresponding residues are K491 and D493 in SARS-CoV RBD). This
174 perfectly explains the B38 specific binding to COVID-19 rather than SARS-CoV.
175 To explore the structural basis for B38 blocking the interaction between COVID-19
176 virus RBD and ACE2, the complex structures of COVID-19 virus RBD/B38-Fab and
177 COVID-19 virus RBD/hACE2 were superimposed. Both the V_H and V_L of B38 result
178 in steric hindrance to the RBD binding to ACE2 (Figure 4C). Notably, the RBDs in
179 B38-bound form and hACE2-bound form exhibit no significant conformational
180 changes with the Cα root mean squared deviation (RMSD) of 0.489 Å (for 194 atoms).
181 Further analysis indicated that 18 of the 21 amino acids on RBD are identical in binding
182 B38 and ACE2 (Figure 4D), which clearly explains why B38 completely abolish the
183 binding between COVID-19 virus RBD and the receptor.
184 COVID-19 virus and SARS-CoV RBDs share relatively high identity, and both of them
185 bind to receptor ACE2 for entry. However, the binding affinities are different. COVID-
186 19 virus RBD exhibits higher binding affinity for receptor binding because of more
187 atomic interactions with hACE2 than that of SARS-CoV RBD. Consequently, the
188 different amino acids located on the hACE2 binding interface may lead to the
189 generation of specific neutralizing antibodies in the host. So far, no antibody has been

190 reported to cross-neutralize both SARS-CoV2 and SARS-CoV by competing the ACE2
191 binding site. CR3022 derived from a convalescent SARS patient can bind to RBDs
192 from both viruses(*18*). However, it enables neutralizing SARS-CoV, but not COVID-
193 19 virus. The epitope of CR3022 does not overlap with the ACE2-binding site(*19*),
194 suggesting that it may be difficult to achieve cross-reactive neutralizing antibodies that
195 can compete with ACE2 binding. A comprehensive understanding of the humoral
196 immune responses against COVID-19 virus should be investigated in more patients. In
197 addition, cocktail antibodies should be considered as an alternative therapeutic strategy
198 to avoid potential escape mutants.
199 As the COVID-19 outbreak continues to spread, characterization of the epitopes on
200 COVID-19 virus RBD protein is essential, which will provide valuable information to
201 develop vaccines. Furthermore, the molecular features of the neutralizing antibodies
202 targeting epitopes are helpful for the development of small molecule or peptide
203 drugs/inhibitors. In conclusion, the neutralizing antibodies identified here are
204 promising candidates for prophylactic and therapeutic treatment against COVID-19
205 virus.
206
207 **References and notes**
208 1. N. Zhu *et al.*, A Novel Coronavirus from Patients with Pneumonia in China,
209 2019. *N Engl J Med*, (2020).
210 2. C. Wang, P. W. Horby, F. G. Hayden, G. F. Gao, A novel coronavirus outbreak
211 of global health concern. *Lancet* **395**, 470-473 (2020).
212 3. P. Zhou, Yang, X.L., Hu, B., Zhang, L., Zhang, W., Si, H.R., Zhu, Y., Li, B.,
213 Chen, J., Luo, H., Guo, H., Jiang, R.D., Liu, M.Q., Chen, Y., Shen, X.R., Wang,

X., Zheng, X.S., Zhao, K., Chen, Q.J., Deng, F., Yan, B., Wang, Y.Y., Xiao, G.F., Shi, Z.L., A pneumonia outbreak associated with a new coronavirus of probable bat origin. *Nature*, (2020).

4. W. Tan *et al.*, Notes from the Field: A novel coronavirus genome identified in a cluster of pneumonia cases-Wuhan, China 2019-2020. *China CDC weekly* **2**, 2 (2020).

5. R. Lu *et al.*, Genomic characterisation and epidemiology of 2019 novel coronavirus: implications for virus origins and receptor binding. *Lancet* **395**, 565-574 (2020).

6. J. F. Chan *et al.*, A familial cluster of pneumonia associated with the 2019 novel coronavirus indicating person-to-person transmission: a study of a family cluster. *Lancet* **395**, 514-523 (2020).

7. F. Wu *et al.*, A new coronavirus associated with human respiratory disease in China. *Nature* **579**, 265-269 (2020).

8. G. Lu, Q. Wang, G. F. Gao, Bat-to-human: spike features determining 'host jump' of coronaviruses SARS-CoV, MERS-CoV, and beyond. *Trends Microbiol* **23**, 468-478 (2015).

9. D. M. Knipe, P. M. Howley, *Fields virology*. (Wolters Kluwer/Lippincott Williams & Wilkins Health, Philadelphia, PA, ed. 6th, 2013), pp. 2 volumes.

10. A. C. Walls *et al.*, Structure, Function, and Antigenicity of the SARS-CoV-2 Spike Glycoprotein. *Cell*, (2020).

11. M. Hoffmann *et al.*, SARS-CoV-2 Cell Entry Depends on ACE2 and TMPRSS2 and Is Blocked by a Clinically Proven Protease Inhibitor. *Cell*, (2020).

12. Q. Wang *et al.*, Structural and Functional Basis of SARS-CoV-2 Entry by Using Human ACE2. *Cell*, (2020).

13. D. Wrapp *et al.*, Cryo-EM structure of the 2019-nCoV spike in the prefusion conformation. *Science* **367**, 1260-1263 (2020).

14. Y. Zhou, Y. Yang, J. Huang, S. Jiang, L. Du, Advances in MERS-CoV Vaccines and Therapeutics Based on the Receptor-Binding Domain. *Viruses* **11**, (2019).

15. L. Du *et al.*, MERS-CoV spike protein: a key target for antivirals. *Expert Opin*

Ther Targets **21**, 131-143 (2017).

16. L. Du *et al.*, The spike protein of SARS-CoV--a target for vaccine and therapeutic development. *Nat Rev. Microbiol* **7**, 226-236 (2009).
17. Q. Wang *et al.*, Neutralization mechanism of human monoclonal antibodies against Rift Valley fever virus. *Nat Microbiol* **4**, 1231-1241 (2019).
18. X. Tian *et al.*, Potent binding of 2019 novel coronavirus spike protein by a SARS coronavirus-specific human monoclonal antibody. *Emerg Microbes & Infect* **9**, 382-385 (2020).
19. M. Yuan *et al.*, A highly conserved cryptic epitope in the receptor-binding domains of SARS-CoV-2 and SARS-CoV. *Science*, (2020).
20. Q. Wang *et al.*, Neutralization mechanism of human monoclonal antibodies against Rift Valley fever virus. *Nat Microbiol* **4**, 1231-1241 (2019).
21. Z. Otwinowski, Minor, W. & Charles W. Carter, Jr. , Processing of X-ray diffraction data collected in oscillation mode. *Methods Enzymol* **276**, 307-326 (1997).
22. P. Emsley, K. Cowtan, Coot: model-building tools for molecular graphics. *Acta Crystallogr D Biol Crystallogr* **60**, 2126-2132 (2004).
23. P. D. Adams *et al.*, PHENIX: building new software for automated crystallographic structure determination. *Acta Crystallogr D Biol Crystallogr* **58**, 1948-1954 (2002).
24. C. J. Williams *et al.*, MolProbity: More and better reference data for improved all-atom structure validation. *Protein Sci* **27**, 293-315 (2018).

Materials and Methods

Ethics statement

All procedures in this study involving authentic COVID-19 virus were performed in biosafety level 3 (BSL-3) facility. Murine studies were performed in an animal biosafety level 3 (ABSL-3) facility. All the procedures in the murine study were

272 reviewed and approved by the Laboratory Animal Welfare and Ethics Committee in
273 Chinese Academy of Sciences. The donor provided written informed consent for the
274 use of blood and blood components followed the approval from the Research Ethics
275 Committee of ShenZhen Third People's Hospital, China.

276 **Cells and Viruses**

277 HEK293T (ATCC CRL-3216) cells and Vero (ATCC CCL-81^{TM}) cells were cultured
278 at 37 °C with 5% CO_2 in Dulbecco's Modified Eagle medium (DMEM) supplemented
279 with 10% fetal bovine serum (FBS). COVID-19 virus strain BetaCoV/shenzhen/SZTH-
280 003/2020 (GISAID ID: EPI_ISL_406594) used in neutralization assay was isolated
281 from the patient in Shenzhen Key Laboratory of Pathogen and Immunity, Shenzhen
282 Third Peoples' Hospital. COVID-19 virus strain HB-01 used in the animal experiment
283 was provided by Professor Wenjie Tan from Chinese center for disease control and
284 prevention. Vero E6 cells were applied to the amplification and titer titration of the
285 virus stocks.

286 **Gene construction**

287 The recombinant protein COVID-19 virus RBD was constructed into two vectors.
288 Residues 331-532 (accession number EPI_ISL_402119) were cloned into pET21a for
289 isolating mAbs as a bait. The coding sequences of COVID-19 RBD (residues 331-532),
290 SARS-CoV RBD (residues 306-527, accession number NC_004718), and hACE2
291 (residues 19-615, accession number BAJ21180) were used in assays of SPR, BLI and
292 crystal screening were constructed into pFastBac1 plasmid with an N-terminal gp67

293 signal peptide and a C-terminal six histidine tag. The pEGFP-N1-hACE2 plasmid was
294 constructed by cloning the coding region into pEGFP-N1 vector using restriction
295 enzymes XhoI and SmaI.

296 **Protein expression and purification**

297 The COVID-19 virus RBD recombinant protein was expressed in *E.coli* as inclusion
298 body and in Bac-to-Bac expression system as soluble protein, respectively. The
299 inclusion body was refolded and further purified by Superdex 200 Hiload 16/60 column
300 (GE Healthcare) in 20 mM Tris, pH 9.0, 150 mM NaCl. Human ACE2 protein was
301 expressed in baculovirus expression system. The constructed pFastBac1 plasmids were
302 transformed into DH10Bac competent cells to generate recombinant bacmids. The
303 bacmids were transfected into Sf9 cells to generate virus and then amplified the virus
304 and infected High five cells for protein expression. Both the soluble COVID-19 virus
305 RBD and hACE2 were purified by HisTrap HP column (GE Healthcare) and were
306 further purified by size-exclusion chromatography with a Superdex 200 column (GE
307 Healthcare) in 20 mM Tris, pH 8.0, 150 mM NaCl.

308 The plasmids of B38 heavy chain and light chain were co-transfected into HEK293T
309 cells to produce B38 IgG. The full-length of B38 were used in neutralization and animal
310 experiments. B38 Fab were generated by papain digestion and further purified by
311 Protein A column (GE Healthcare) as described before(*20*).

312 **Bio-Layer Interferometry (BLI)**

313 The antibody binding screening and the competitive binding of mAbs and hACE2 (or
314 between two antibodies) were measured by BLI using the Octet RED96 system

315 (FortéBio). All experiments were performed at 25 °C, and the biosensors were pre-
316 equilibrated in a buffer containing 20 mM HEPES, pH7.4 and 150 mM NaCl and 0.005%
317 (v/v) Tween-20 for 10min. For the antibody binding screening assay, 293T cell derived
318 antibodies supernatants were loaded onto AHC biosensors for 120 s and flowed with
319 500 nM COVID-19 virus RBD or 1μM SARS-CoV RBD. To determine the competitive
320 characteristics, 10 μg/mL biotinylated COVID-19 virus RBD was loaded onto
321 streptavidin biosensors for 60 s, and flowed 300 nM of the first protein (one antibody)
322 for 240 s and the second protein (hACE2 or the second antibody) for 240 s. The
323 interference patterns from the biotinylated RBD with buffer and the uncoated
324 biosensors with protein were analyzed as two sets of controls. We used corrected data
325 to compare the competitive characteristics by Octet data analysis software.

326 **Surface plasmon resonance (SPR)**

327 The affinity between COVID-19 virus RBD and antibodies were measured at room
328 temperature using a BIAcore 8K system. All proteins used for kinetic analysis were
329 exchanged to the buffer of 20 mM HEPES, 150 mM NaCl, pH 7.4 and 0.005% (v/v)
330 Tween-20. A CM5 chip (GE Healthcare) was coupled with anti-human Fc antibody to
331 capture the antibodies at 8000 response units. Gradient concentrations of COVID-19
332 virus RBD (from 200 nM to 12.5 nM with 2-fold dilution) were then flowed over the
333 chip surface. After each cycle, the sensor surface was regenerated with Gly-HCl pH1.7.
334 The affinity was calculated with BIAevaluation software.

335 **Crystal screening and structure determination**

336 The COVID-19 virus RBD protein and B38-Fab fragment were mixed at a molar ration

337 of 1:1.2. The mixture was incubated on ice for 60 min and further purified by Superdex-
338 200 column (GE Healthcare). 5 mg/mL and 10 mg/mL of hCoV-19 RBD/B38 Fab
339 proteins were used for crystal screening by vapor-diffusion sitting-drop method at 18°C.
340 Diffracting crystals were obtained in the condition consisting of 0.15 M ammonium
341 sulfate, 0.1 M MES pH 6 and 15% w/v PEG 400. Diffraction data were collected at
342 Shanghai Synchrotron Radiation Facility (SSRF) BL17U (wavelength, 0.97919 Å).
343 The crystals were cryo-protected by briefly soaking in reservoir solution supplemented
344 with 20% (v/v) glycerol before flash-cooling in liquid nitrogen. The dataset was
345 processed with HKL2000 software(*21*). The complex structure was determined by the
346 molecular replacement method using Phaser with our previously reported hCoV-2 RBD
347 structure (PDB code, 6LZG) and Fab structure (PDB code, 4TSA). The atomic models
348 were completed with Coot(*22*) and refined with phenix.refine in Phenix(*23*), and the
349 stereochemical qualities of the final models were assessed with MolProbity(*24*). Data
350 collection, processing, and refinement statistics are summarized in Table S1. All the
351 figures were prepared with Pymol software (http://www.pymol.org).

352 **Neutralization assay**

353 10^4 Vero cells were seeded in a 96-well plate (Costar) per well 24 hours before infection.
354 On the day of infection, the cells were washed twice with PBS. Each mAb was diluted
355 2-fold in cell culture medium (modified eagle medium). 40 μL of diluted mAb (100
356 μg/mL as initial concentration) was added to 40 μL of cell culture medium containing
357 100 times the tissue culture infective dose ($TCID_{50}$) of the BetaCoV/Shenzhen/SZTH-
358 003/2020 strain virus on a 96-well plate in decuplicate and incubated at 37 °C for 2

359 hours. The mixture was then added to cells and incubated at 37 °C. The cytopathic
360 effect was examined for 5 days post-infection. The complete absence of cytopathic
361 effect in an individual culture well was defined as protection. The values of IC_{50} were
362 calculated using prism software (GraphPad).

363 **Animal experiments**

364 Twelve female hACE2 transgenic mice (5-6 weeks old) were divided into three groups
365 with four mice in each group. All the mice were anaesthetized with thibromoethanol
366 and then intranasally inoculated with 50μL 1×10^5 $TCID_{50}$ COVID-19 virus (HB-01).
367 After 12 hours, mice received a dose of 25 mg/kg B38 or H4 i.p. in a volume of 100
368 μL, an equivalent volume of PBS was administered as a control. Body weights were
369 monitored and recorded for four days. All the mice were euthanized at 3 dpi. The lung
370 homogenates were prepared in 1 mL DMEM and then centrifuged at 3000 rpm for 10
371 min at 4 °C. The supernatant was collected to extract viral RNA by using the QIAamp
372 Viral RNA Mini Kit (Qiagen). RNA was eluted in 80 μL elution buffer, and 5 μL was
373 taken as the template for the quantitative real-time reverse transcription-PCR (qRT-
374 PCR) by rRT-PCR kit (Mabsky Biotech Co., Ltd., CONFORMITE EUROPEENNE NO.
375 DE/CA20/IVD-luxuslebenswelt-68/20). The primers targeting N gene were used as
376 followed: F: 5'-ATTGGCATGGAAGTCACACCTTC-3', R: 5'-
377 TGCTTATTCAGCAAAATGACTTGAT-3', probe: FAM--
378 TGGTTGACCTACACAGGTGCCATCA--BHQ1. The amplification was performed
379 as followed steps: 50 °C for 30 min, 95 °C for 3 min, followed by 45 cycles at 95 °C 5
380 s and 55 °C for 30 s. This mice model was established and supplied by Institute for

Laboratory Animal Resources, NIFDC.

Acknowledgements

We thank the staff of the BL17U1 beamline at Shanghai Synchrotron Radiation Facility (SSRF) for data collection. This work was supported by Zhejiang University special scientific research fund for COVID-19 prevention and control (2020XGZX019), the National Science and Technology Major Project (2018ZX10733403), the National Key R&D Program of China (2018YFC1200603), the National Key Plan for Scientific Research and Development of China (2016YFD0500304), National Natural Science Foundation of China (31872745 and 81902058), and the National Science and Technology Major Projects of Infectious Disease Funds (2017ZX10304402).

Author contributions

Y.W., F.G., G.F.G. and L.L. initiated and coordinated the project. Y.W., F.G. and G.F.G designed the experiments. Y.L. and L.L. provided the convalescent PBMCs. Y.W. and C.S performed the cell sorting. W.P., C.Z, Z.L. and C.G.S. sequenced and constructed the antibodies. Y.W. conducted the SPR and Octet analysis with the help of F.Z., F.W., Z.L. and Q.W.. C.S. and Y.Y. evaluated the neutralizing potency. S.L. and Y.B. conducted the animal experiments with the help from G.W., W.T., X.L. C.F. and H.X.. qRT-PCR was conducted by Y.G.. F.W., W.P. D.L. C.Z. and Z.L expressed and purified proteins. J.Q. and F.G. collected the diffraction dada and determined the complex structure. Y.W., F.G. and G.F.G. analyzed the data and wrote the manuscript. S.T. revised the manuscript.

Competing interests

404 Y.W., F.W., C.S., D.L., S.T., Y.L, G.F.G and L.L. are listed as inventors on pending
405 patent applications for mAb B38 and H4. The other authors declare that they have no
406 competing interests.

407 **Data availability statements**

408 All the data and reagents presented in this study are available from the corresponding
409 authors upon request.

410 **Figure legends**

411 **Figure 1. Characterization of COVID-19 virus specific neutralizing antibodies.** (A-
412 D) The binding kinetics of the four antibodies (B38, H4 B5 and H2) with COVID-19
413 virus RBD were measured by using a single-cycle BIAcore 8K system. The antibodies
414 were captured on a CM5 chip coupled with anti-human Fc antibody. The COVID-19
415 RBD was serially diluted and injected with single-cycle kinetics procedure. The binding
416 affinity (Kd) was labeled accordingly. (E-H) Competition binding to the COVID-19
417 virus RBD between antibody and ACE2 was measured by BLI in OctetRed96.
418 Biotinylated COVID-19 virus RBD (10 μg/mL) were immobilized on SA sensors. The
419 SA sensors were saturated with antibodies, and then flowed with corresponding
420 antibody in the presence of 300 nM soluble ACE2 (blue) or without ACE2 (red). As a
421 control, the immobilized biotinylated COVID-19 virus RBD was first flowed with
422 buffer, and then flowed with the equal molar of ACE2 (black). (I) hACE2-EGFP was
423 expressed on the HEK293T cell surface, and the cells were stained with 200 ng/mL
424 COVID-19 virus RBD his-tag proteins pre-incubated with isotype IgG, B38, H4, B5 or
425 H2. The percentage of both anti-histag APC^+ and $EGFP^+$ cells were calculated. (J-K)

426 Competition binding to COVID-19 virus RBD between B38 and H4 was measured by
427 BLI. Immobilized COVID-19 virus RBD (10 μg/mL) were saturated with 300 nM of
428 the first antibody, and then flowed with equal molar of the first antibody in the presence
429 of (blue) or without (red) the second antibody. As a control, the immobilized COVID-
430 19 RBD was first flowed with buffer, and then flowed with the second antibody (black).
431 **Figure 2. Four antibodies can effectively neutralize COVID-19 virus.** The mixtures
432 of SARS-CoV-2 and serially diluted antibodies were added to Vero E6 cells. After 5
433 days incubation, IC_{50} were calculated by fitting the CPE from serially diluted antibody
434 to a sigmoidal dose-response curve. The IC_{50} were labeled accordingly.
435 **Figure 3. The protection efficiency of mAbs in hACE2 mice model post infection**
436 **with COVID-19 virus.** (A) Body weight loss were recorded for PBS (n=4), B38
437 treatment (n=4) and H4 treatment (n=4) groups. All the mice were challenged
438 intranasally with COVID-19 virus, and 25 mg/kg antibodies were injected (i.p.) 12
439 hours post-infection. Equal volume of PBS was used as a control. The weight loss was
440 recorded over three days, and the significant difference can be observed between B38
441 group and PBS group (unpaired *t*-test, ***$p<0.001$). (B) The virus titer in lungs of three
442 groups were determined at 3 dpi by qRT-PCR. The mAb treatment group can reduce
443 the viral load in the lung of mice (unpaired *t*-test, ***$p<0.001$).
444 **Figure 4. Structural analysis of B38 and COVID-19 virus RBD complex and the**
445 **epitope comparison between B38 and hACE2.** (A) The overall structure of B38 Fab
446 and COVID-19 virus RBD complex. The B38 heavy chain (cyan), light chain (green)
447 and COVID-19 virus RBD (magenta) are displayed in cartoon representation. (B) The

epitope of B38 are shown in surface representation. The contacted residues by heavy chain, light chain or both are colored in cyan, green and magenta, respectively. The identical residues on RBD involved in binding to both B38 and hACE2 are labeled in red. (C) Superimposition of B38/COVID-19 virus RBD and hACE2/COVID-19 virus RBD (PDB: 6LZG). All the molecules are presented in cartoon, with the same colors in panel A. hACE2 is colored in light pink. (D) The residues involved in hACE2-RBD binding are highlighted in light pink. The identical residues on RBD involved in binding to both B38 and hACE2 are labeled in red. (E) The complex structure of SARS-CoV RBD (light blue) and hACE2 (yellow) (PDB:2AJF). (F) The residues of SARS-CoV RBD in contact with hACE2 are colored in yellow. The residues are numbered according to SARS-CoV RBD. The identical residues involved in hACE2 binding of two RBDs are labeled in red. (G-I) The detailed interactions between COVID-19 virus RBD and HCDR loops. (J-K) The detailed interactions between COVID-19 virus RBD and LCDR loops. The residues are shown in sticks with the identical colors to figure 3C. The water molecules are displayed in red sphere.

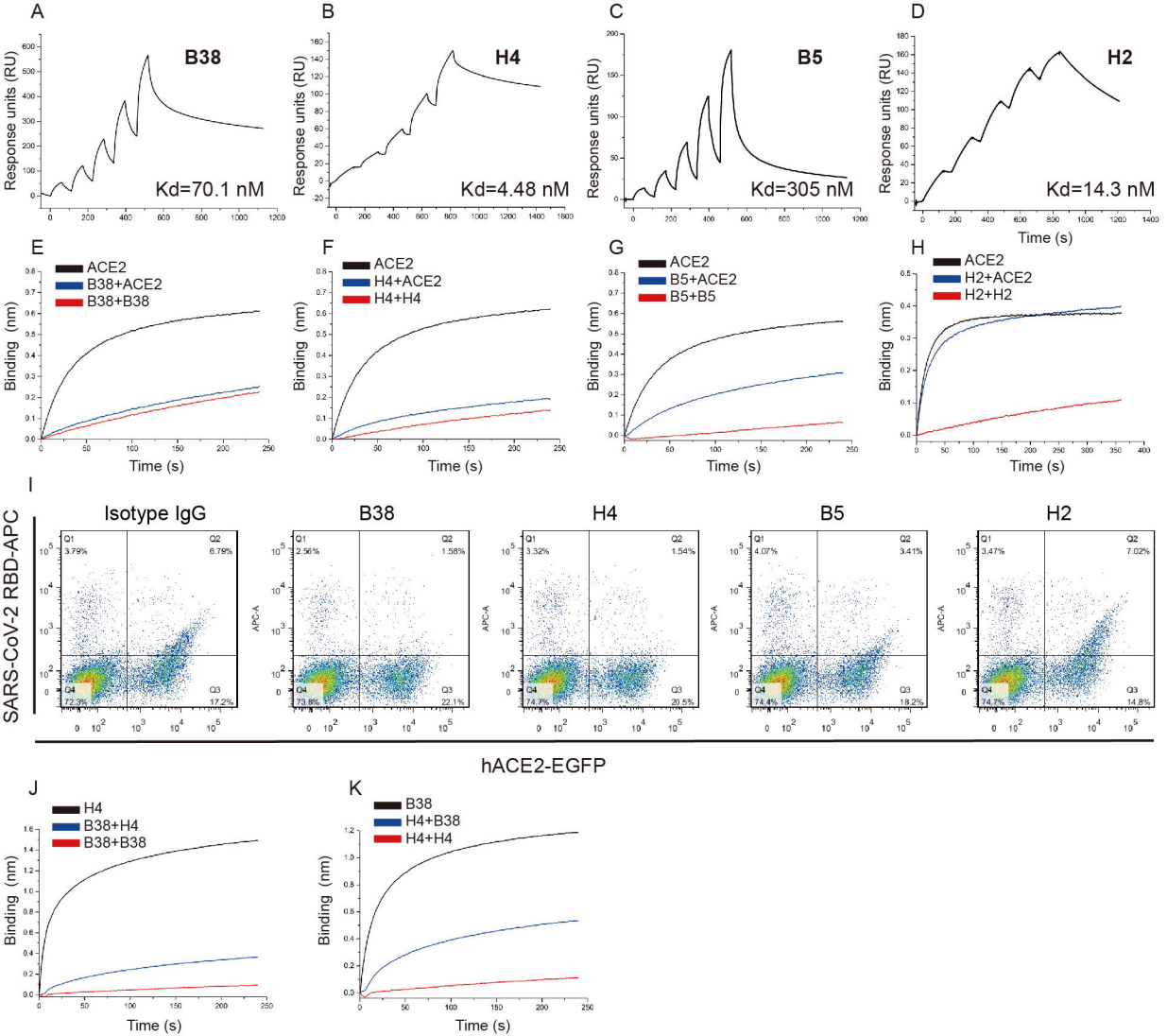
A
B38
Kd=70.1 nM
Response units (RU)
B
H4
Kd=4.48 nM
Response units (RU)
C
B5
Kd=305 nM
Response units (RU)
D
H2
Kd=14.3 nM
Response units (RU)
Time (s)
E
ACE2
B38+ACE2
B38+B38
Binding (nm)
Time (s)
F
ACE2
H4+ACE2
H4+H4
Binding (nm)
Time (s)
G
ACE2
B5+ACE2
B5+B5
Binding (nm)
Time (s)
H
ACE2
H2+ACE2
H2+H2
Binding (nm)
Time (s)
I
Isotype IgG
B38
H4
B5
H2
SARS-CoV-2 RBD-APC
hACE2-EGFP
APC-A
Q1 3.79%
Q2 6.79%
Q4 72.3%
Q3 17.2%
Q1 2.56%
Q2 1.58%
Q4 73.8%
Q3 22.1%
Q1 3.32%
Q2 1.54%
Q4 74.7%
Q3 20.5%
Q1 4.07%
Q2 3.41%
Q4 74.4%
Q3 18.2%
Q1 3.47%
Q2 7.02%
Q4 74.7%
Q3 14.8%
J
H4
B38+H4
B38+B38
Binding (nm)
Time (s)
K
B38
H4+B38
H4+H4
Binding (nm)
Time (s)

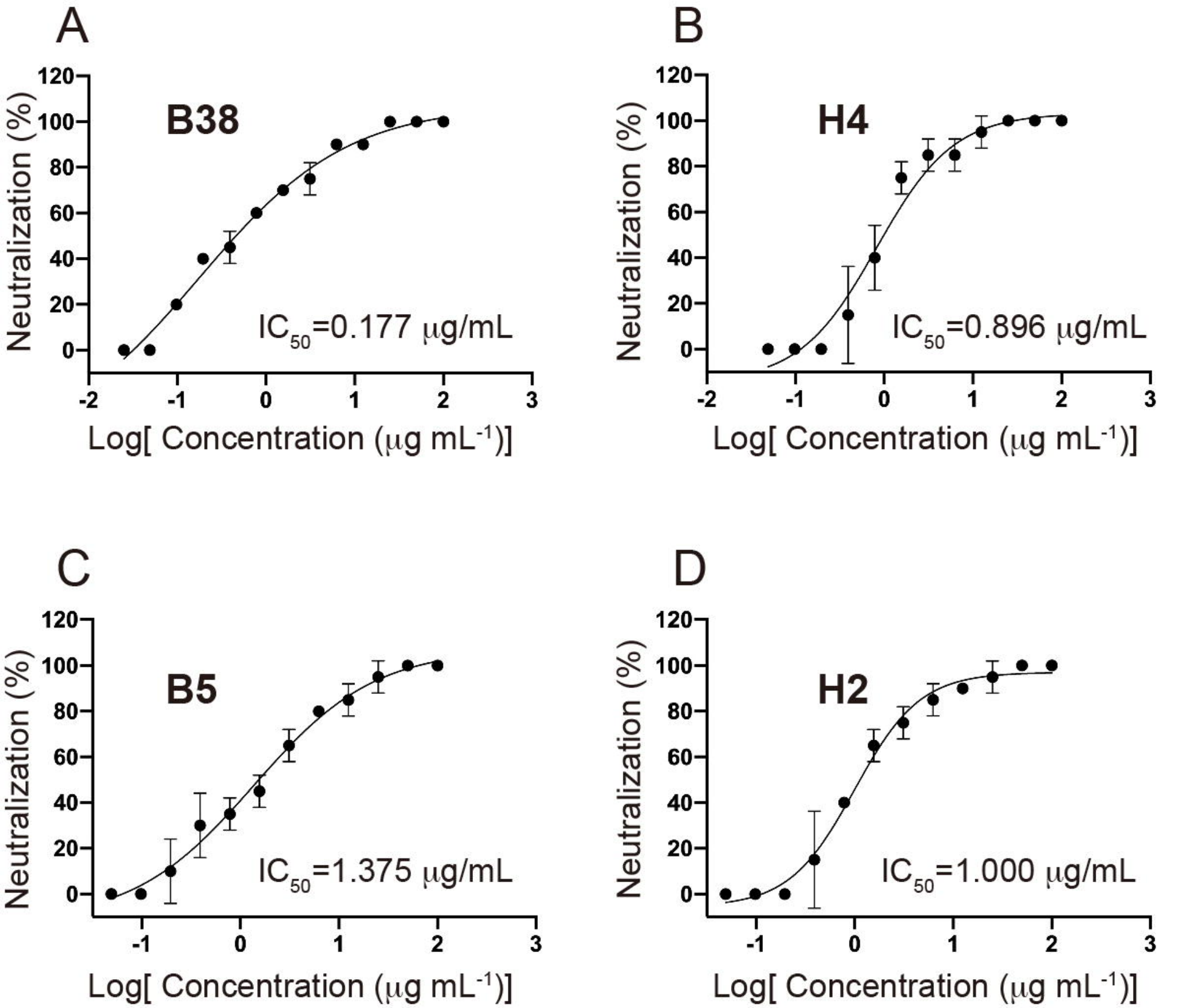
A
B38
IC50=0.177 μg/mL
Neutralization (%)
Log[Concentration (μg mL-1)]
B
H4
IC50=0.896 μg/mL
Neutralization (%)
Log[Concentration (μg mL-1)]
C
B5
IC50=1.375 μg/mL
Neutralization (%)
Log[Concentration (μg mL-1)]
D
H2
IC50=1.000 μg/mL
Neutralization (%)
Log[Concentration (μg mL-1)]

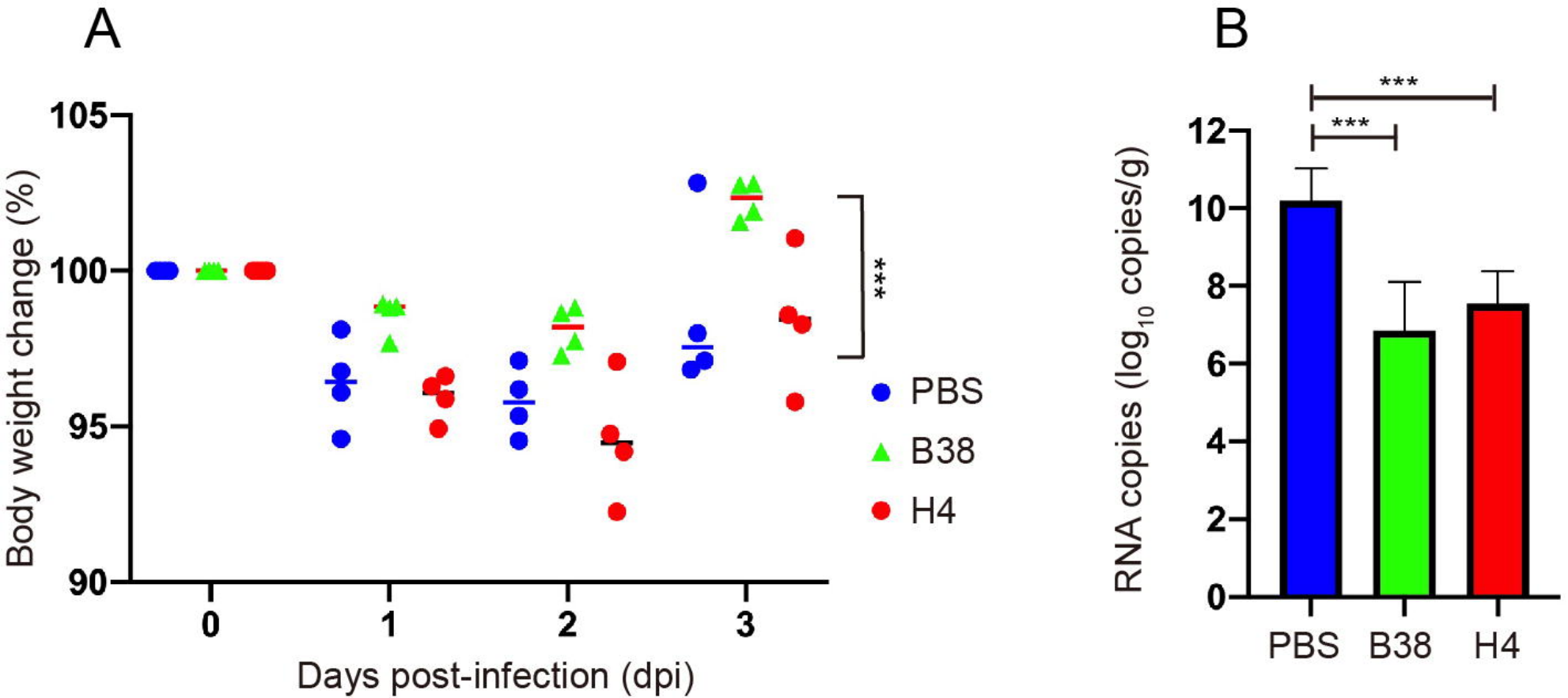
A
105
100
95
90
Body weight change (%)
0
1
2
3
Days post-infection (dpi)
***
PBS
B38
H4
B
***
***
12
10
8
6
4
2
0
RNA copies (log10 copies/g)
PBS
B38
H4

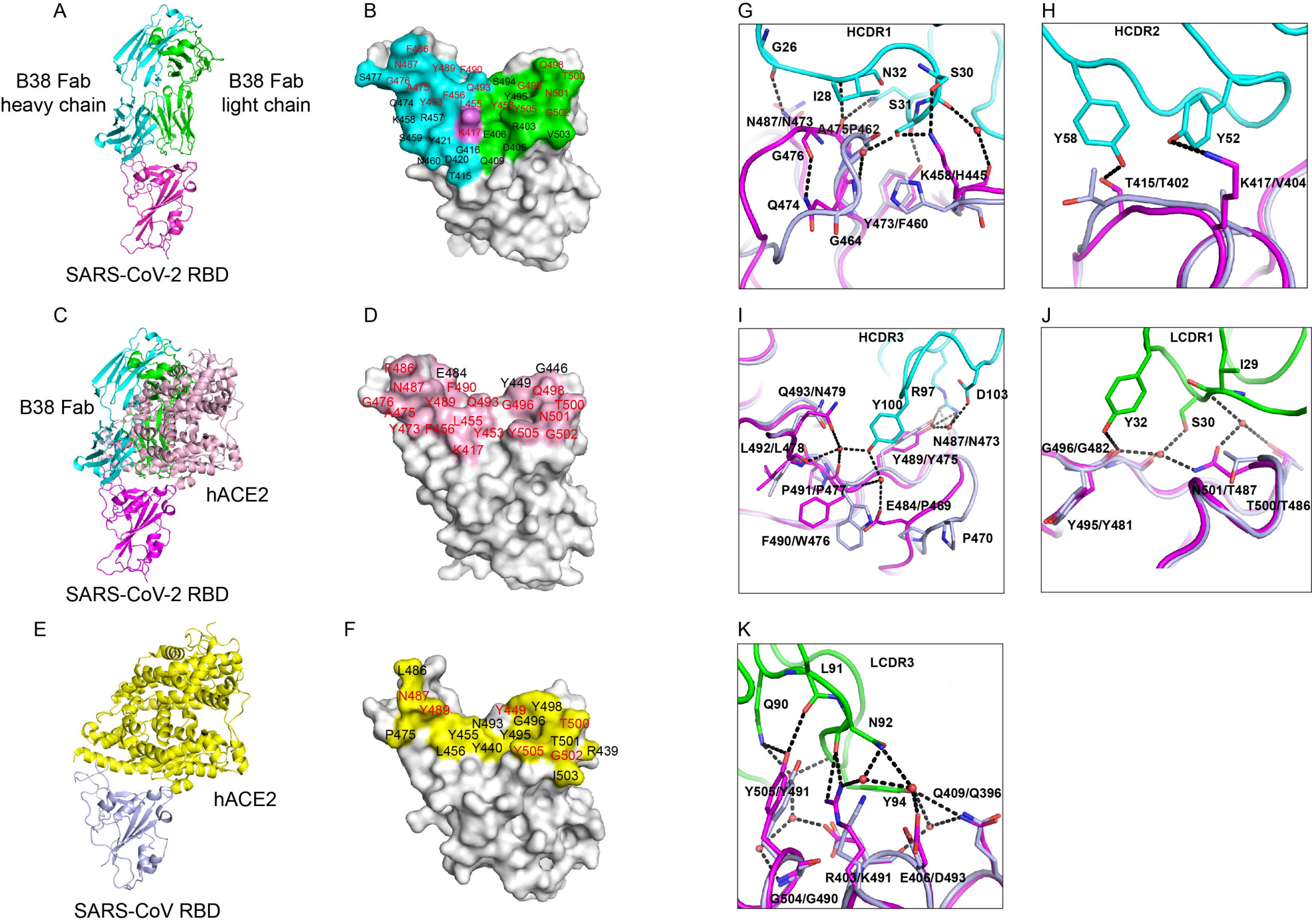
A
B38 Fab heavy chain
B38 Fab light chain
SARS-CoV-2 RBD
B
F486
N487
Y489
F490
Q498
T500
S477
G476
A475
Q493
S494
G496
N501
Q474
Y473
F456
L455
Y495
Y453
Y505
G502
K458
R457
K417
E406
R403
V503
S459
Y421
G416
D405
N460
D420
Q409
T415
C
B38 Fab
hACE2
SARS-CoV-2 RBD
D
F486
E484
G446
N487
F490
Y449
Q498
G476
Y489
Q493
G496
T500
A475
L455
N501
Y473
F456
Y453
Y505
G502
K417
E
hACE2
SARS-CoV RBD
F
L486
N487
Y489
Y449
Y498
N493
G496
T500
P475
Y455
Y495
T501
L456
Y440
Y505
G502
R439
I503
G
HCDR1
G26
N32
S30
I28
S31
N487/N473
A475
P462
G476
K458/H445
Q474
Y473/F460
G464
H
HCDR2
Y58
Y52
T415/T402
K417/V404
I
HCDR3
Q493/N479
R97
D103
Y100
N487/N473
L492/L478
Y489/Y475
P491/P477
E484/P469
F490/W476
P470
J
LCDR1
I29
Y32
S30
G496/G482
N501/T487
T500/T486
Y495/Y481
K
LCDR3
L91
Q90
N92
Y505/Y491
Y94
Q409/Q396
R403/K491
E406/D493
G504/G490